

Grid cell distortion is associated with increased distance estimation error in polarized environments

Highlights

- Distance estimation is impaired in trapezoids, but not rectangles, in rats and humans
- Grid cell symmetry is distorted in trapezoidal, but not rectangular, environments
- Grid cell distortion is correlated with distance estimation error
- Experience of a trapezoid distorts grid cell symmetry in future experiences

Authors

Stephen Duncan, Maneesh V. Kuruvilla,
Benjamin Thompson, Daniel Bush,
James A. Ainge

Correspondence

jaa7@st-andrews.ac.uk

In brief

Duncan et al. demonstrate that distance estimation is impaired in polarized environments like trapezoids relative to regular rectangular environments. Grid cells recorded in the trapezoid environment are distorted, and the level of distortion correlates with distance estimation error. Trapezoid-induced distortion is partially maintained in future experiences in the rectangle.

Report

Grid cell distortion is associated with increased distance estimation error in polarized environments

Stephen Duncan,^{1,2,5} Maneesh V. Kuruvilla,^{1,3,5} Benjamin Thompson,¹ Daniel Bush,⁴ and James A. Ainge^{1,*}

¹School of Psychology and Neuroscience, University of St Andrews, St Mary's Quad, South Street, St Andrews KY16 9JP, UK

²Department of Psychology & Brain Sciences, Indiana University, 1101 E. 10th Street, Bloomington, IN 47405, USA

³Wicking Dementia Research Centre, University of Tasmania, 17 Liverpool Street, Hobart, TAS 7001, Australia

⁴Department of Neuroscience, Physiology, and Pharmacology, University College London, Gower Street, London WC1E 6BT, UK

⁵These authors contributed equally

*Correspondence: jaa7@st-andrews.ac.uk

<https://doi.org/10.1016/j.cub.2025.08.011>

SUMMARY

Grid cells within the medial entorhinal cortex (MEC) exhibit a regular hexagonal pattern of firing fields,¹ which has been hypothesized to provide a universal spatial metric, supporting spatial memory and navigation. This could be used to support a cognitive map, our internal representation of external space,^{2–6} and consistent with this, disruption of the MEC impairs spatial memory and place cell anchoring to external visual cues.^{7–10} However, the highly regular and repetitive nature of the firing fields in grid cells is also ideally suited to support path integration.^{11–17} Indeed, genetic silencing of stellate cells in MEC results in impaired distance estimation, supporting the MEC's role in path integration.¹⁸ However, few studies have examined the role of grid cell firing during active navigation. Several studies have reported that manipulation of environmental cues, recent experience, and reward location distort the grid signal,^{19–25} but most relevant here is that the grid signal distorts in polarizing environments, such as trapezoids.^{26,27} If grid cells support distance estimation and path integration, then disruption of the grid regularity, such as that seen in polarized environments, should impair these processes. Here, we report that both rats and humans have impaired distance estimation in polarized environments. Grid regularity was again reported to be distorted in polarized environments, and this was correlated with impaired distance estimation in rats. Grid regularity was also distorted by recent experience. These findings are consistent with grid cells supporting distance estimation in navigation.

RESULTS AND DISCUSSION

To examine path integration, we trained rats and humans to carry out a distance estimation task in a regular shaped rectangular environment. We then changed the shape of the environment to a trapezoid and examined the effect that this had on distance estimation. Next, we examined the proposed role of grid cells in distance estimation by recording grid cells in the rectangle and trapezoid as rats carried out the distance estimation task. We predict that regularity of grid firing will be related to accurate distance estimation and that both grid regularity and accuracy of distance estimation will decrease in polarized environments.

Distance estimation is impaired in rats and humans in polarized environments

Rats ($n = 21$) were trained on a distance estimation task within a rectangular environment in 2 cohorts ($n = 16$ behavior, $n = 5$ electrophysiology). A start box was attached to one end of the box, and on each trial, rats were rewarded for leaving the start box, running a specific distance, and then returning to the start box. Initial training used rewards at the required stopping position, but overtrained rats were exposed to increasingly frequent

trials where the required distance was not baited. Once rats could complete 10 unbaited trials in a day, they progressed to the main testing phase of the study. In this phase, rats ran the same distance estimation task, but in half of the trials, the box was transformed into a trapezoid, while in the other half, the box was the standard rectangular shape (Figure 1A). Distance estimation was significantly different in the trapezoid relative to the rectangle trials, with animals consistently overestimating (Figure S1A) the distance they have run and stopping short of the reward in the trapezoid (Figure 1B; $F_{(1, 15)} = 189.623$, $p < 0.001$). Distance estimation error as measured by distance from the reward point was also significantly increased in the trapezoid (Figure 1C; $F_{(1, 15)} = 47.12$, $p < 0.001$). Examination of individual trajectories shows that in most trials rats ran straight to the reward and then followed a more circuitous route back to the start box (Figure S1B). Running speed did not differ between rectangle and trapezoid trials ($t_{(4)} = -0.549$, $p = 0.612$; Figure S1C). This shows that accurate distance estimation is dependent on environmental geometry and impaired in polarized environments. Interestingly, the environment was surrounded by distal cues outside of the box in both types of trial. While these were clearly not sufficient to support accurate distance

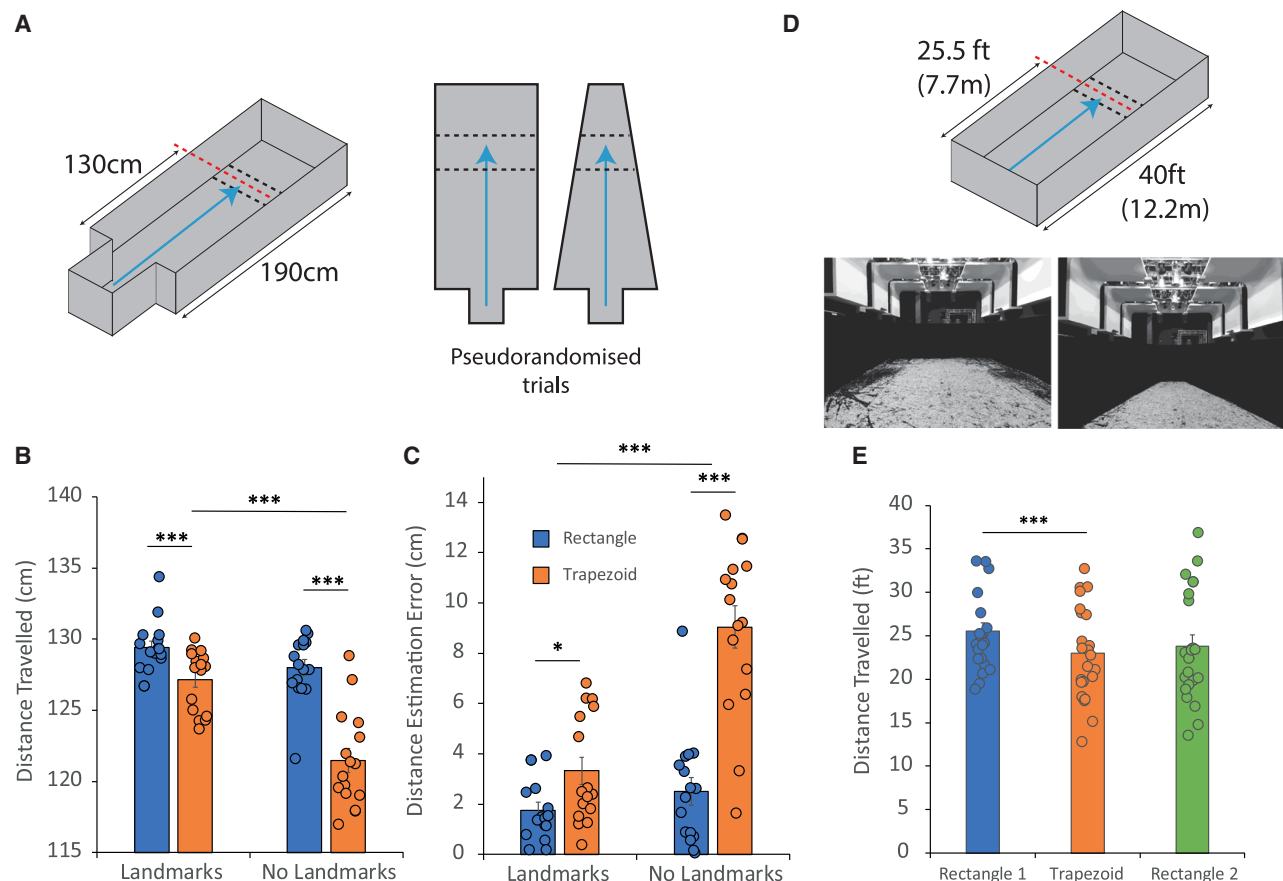


Figure 1. Rats and humans overestimate distance traveled in the trapezoid-shaped environment

(A) Diagram detailing the dimensions of the rat testing box alongside its rectangular and trapezoidal configurations. Black dashed lines indicate the boundaries of the reward zone, with the red dashed line indicating the center of the reward zone. The blue arrow indicates the intended path of travel from the starting box to the reward zone.

(B) Mean distance traveled by rats ($n = 16$) in the rectangle (blue) and trapezoid (orange) environments with or without landmarks visible.

(C) Mean absolute distance estimation error in the rectangle (blue) and trapezoid (orange) environments with or without landmarks visible.

(D) Diagram (top) and representative photos (bottom) of the apparatus used in the human version of the distance estimation task in both its rectangular (left) and trapezoidal (right) configurations.

(E) Mean distance traveled by human participants ($n = 23$) in the first rectangle, trapezoid, and second rectangle configurations.

* $p < 0.05$, *** $p < 0.001$. Error bars indicate \pm SEM.

See also Figure S1.

estimation by themselves, they could help to correct errors in distance estimation caused by the change in environment geometry. To examine this, we removed distal cues by surrounding the arena with a curtain. Distance estimation without distal cues was even more severely affected, with rats' overestimation of the distance traveled in the trapezoid being even more profound in this condition (Figures 1B and 1C; distance traveled – $F_{(1, 15)} = 189.623$, $p < 0.001$; distance estimation error – $F_{(1, 15)} = 47.12$, $p < 0.001$).

To test whether this effect is also present in humans, a version of the apparatus was produced at a scale that allowed human testing in the real world (Figure 1D). Taking account of the difference in average stride length between rats and humans, the human version of the box was 12.2 m long and 6.1 m wide. All other features of the box were maintained, including the ability to change the rectangle into a trapezoid. Human participants

($n = 23$) were given similar habituation and training trials and then tested on distance estimation in rectangle and trapezoid trials. Due to time constraints associated with transforming the arena between geometric configurations, trials were run in blocks of rectangle, trapezoid, and then rectangle. Humans showed good distance estimation in the rectangle and also the same pattern of distance overestimation in the trapezoid, stopping significantly short of the required distance ($F_{(1, 445, 31.779)} = 8.534$, $p < 0.01$; Figure 1E). Post hoc comparisons revealed that participants showed the same pattern of behavior as the rats by overestimating distance in the trapezoid. Interestingly, the number of steps ($F_{(1, 445, 31.779)} = 1.959$, $p = 0.153$; Figure S1D) and average time to complete trials ($F_{(1, 445, 31.779)} = 1.329$, $p = 0.275$; Figure S1E) were not different between conditions, but speed was significantly higher in the first block of rectangle trials relative to other blocks ($F_{(1, 445, 31.779)} = 20.13$, $p < 0.001$; Figure S1F).

Current Biology Report

CellPress
OPEN ACCESS

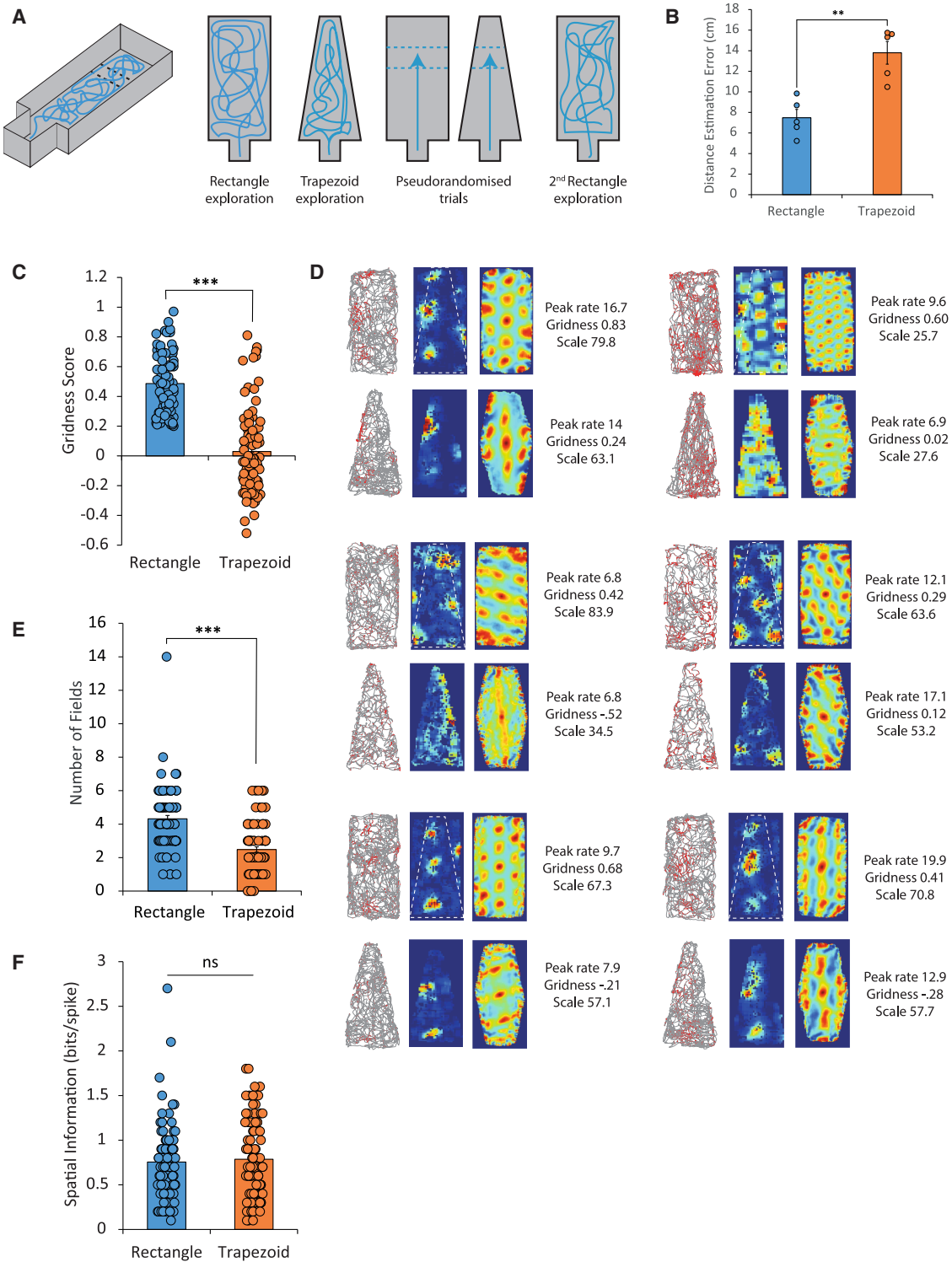


Figure 2. Decreased grid regularity in the trapezoid

(A) Diagram showing the stages of the distance estimation task (left to right) for implanted rats.

(B) Mean absolute distance estimation accuracy for the implanted rats ($n = 5$) in the rectangle (blue) and trapezoid (orange) trials.

(C) Mean gridness score of grid cells ($n = 85$) in the rectangle and trapezoid open fields.

(D) Spike maps, rate maps, and autocorrelations (left to right) for grid cells in the rectangle (upper) and trapezoid (lower) open fields. Dashed white lines show the outline of the trapezoid on the rectangle maps for reference.

(legend continued on next page)

Participants also reported feeling less confident in their distance estimation in the trapezoid relative to the rectangle ($F_{(1,445, 31,779)} = 17.22, p < 0.001$; **Figure S1G**). This raises interesting questions regarding how top-down cognitive processes, such as confidence may affect behavior and spatial representations. Studies directly examining grid cell activity and confidence in humans could address these issues.

Grid cell regularity is disrupted in the trapezoid

To examine grid cell regularity in polarized environments, we recorded from medial entorhinal cortex (MEC) in 5 rats as they explored the rectangle- and trapezoid-shaped boxes (**Figures 2A** and **S2A**). Rats were initially run in an open field session in both the rectangle and trapezoid configurations to allow comparison of grid cell characteristics between shapes. Rats were then run through the distance estimation task in both shapes before a final open field session in the rectangle (**Figure 2A**). Rats in the electrophysiology group showed the same pattern of distance estimation as those from the behavioral study, with significant overestimation of distance traveled in the trapezoid relative to the rectangle ($t_{(4)} = 6.45, p = 0.003$; **Figure 2B**). We recorded 444 cells from MEC, 85 of which passed standard shuffling-based procedures to be classed as grid cells (**Figure S2B**). Consistent with previous reports, grid cell regularity was significantly reduced in the trapezoid relative to the rectangle (**Figures 2C** and **S2C**; $W = 90.5, p < 0.001$). Examples of grid cells in **Figure 2D** show similar patterns to previously reported ones, where grid cell regularity is particularly disrupted at the narrow end of the box. Consistent with this, the average number of firing fields was significantly lower in the trapezoid relative to the rectangle (**Figure 2E**; $W = 155.5, p < 0.001$), although levels of spatial information were not affected (**Figure S2F**; $W = 1,148.5, p = 0.197$). One possible explanation for these changes is that they may be the result of sampling from a smaller environment. To examine this possibility, we reanalyzed the rate maps from the rectangle session with an appropriately sized trapezoid-shaped mask. The number of fields ($\chi^2_{(2)} = 62.49, p < 0.001$) and gridness scores ($\chi^2_{(2)} = 84.99, p < 0.001$) for the masked rectangles were significantly lower than in the rectangle but critically were significantly higher than they were in the trapezoid (**Figures S3A** and **S3B**). Information score remained unaffected across all conditions ($\chi^2_{(2)} = 3.228, p = 0.199$; **Figure S3C**). This shows that reducing the area of the environment does affect gridness and the number of fields in grid cells but does not account for all of the changes induced by the trapezoid.

Decreased grid regularity is associated with increased distance estimation error

To examine the hypothesis that impaired grid cell regularity might underlie distance estimation error, we recorded from grid cells as animals carried out the distance estimation task in both the rectangle and the trapezoid tasks (**Figure 2A**). Grid cell regularity is impossible to assess in single-trajectory trials using traditional measures such as gridness, which require

complete coverage of an environment to produce a firing rate map from which spatial autocorrelations are calculated. However, the regularity of grid cell firing allows predictions to be made about the relative distances between spikes even on single trajectories. Spikes within a grid field should have low inter-spike distances, while spikes in different grid fields will have much greater distances between them (**Figure 3A**). Further, the distances between spikes in different fields should form regular peaks when plotted against distance traveled by the rat (**Figure 3B**). To examine the regularity of grid firing, we created interspike distance firing rate plots for the open field sessions in both the rectangle and trapezoid. These showed clear peaks in firing rate, which correspond to the scale or phase of the grid cell in that session (**Figure 3C**). To determine if these interspike distance firing rate plots were able to assess grid distortion, we measured the average distances between the peaks in these plots for each of the grid cells in the open fields. We observed significant reductions in the inter-peak distances in the trapezoid compared with the rectangle open field for both the first 2 peaks and an average of all peaks in the distribution (**Figure 3D**; $W_{(63)} = 542.5, p = 0.001$; **Figure 3E**; $W_{(63)} = 463, p < 0.001$), indicating that these plots were also able to detect disruption in grid regularity associated with the trapezoid. This reduction in distance between peaks could be consistent with the distortion being at least partially due to a rescaling of the original map. However, rescaling by itself would preserve grid regularity, and so we would expect the gridness scores to still be high. The significant reduction in gridness in both the trapezoid and masked rectangle argues against this.

Next, we examined interspike distance in the distance estimation trials. To determine whether grid cell firing was disrupted in the trials, we compared interspike distance distributions from the trials to the distributions from the open field session (**Figure 3F**). Differences between these distributions give a measure that takes into account changes in firing rate and distance between peaks in the distributions from different sessions (trials vs. open field) and so can be used as a proxy for grid distortion that encompasses both rate and spatial change in the grid signal. The number of spikes fired on any given trial was variable and depended largely on whether rats ran trajectories that passed through grid fields. Consequently, not all grid cells identified in the open field sessions could be analyzed, but 67 out of 85 recorded grid cells fired sufficient spikes in the trial trajectories to allow for this measure. Grid disruption in the rectangle trials (relative to the rectangle open field) was low, whereas disruption in the trapezoid trials was significantly increased relative to either the rectangle or trapezoid open field sessions. This shows that, consistent with the open field sessions, grid regularity was significantly lower in the trapezoid relative to the rectangle trials (**Figure 3G**; $H_{(2)} = 49.79, p < 0.001$). Critically, the behavioral effect reported in **Figure 1** is reproduced in the animals from which grid cells were recorded, who again showed significantly increased distance estimation error in the trapezoid relative to the rectangle. To examine whether there is any association

(E) Mean number of fields for grid cells in the rectangle and trapezoid open fields.

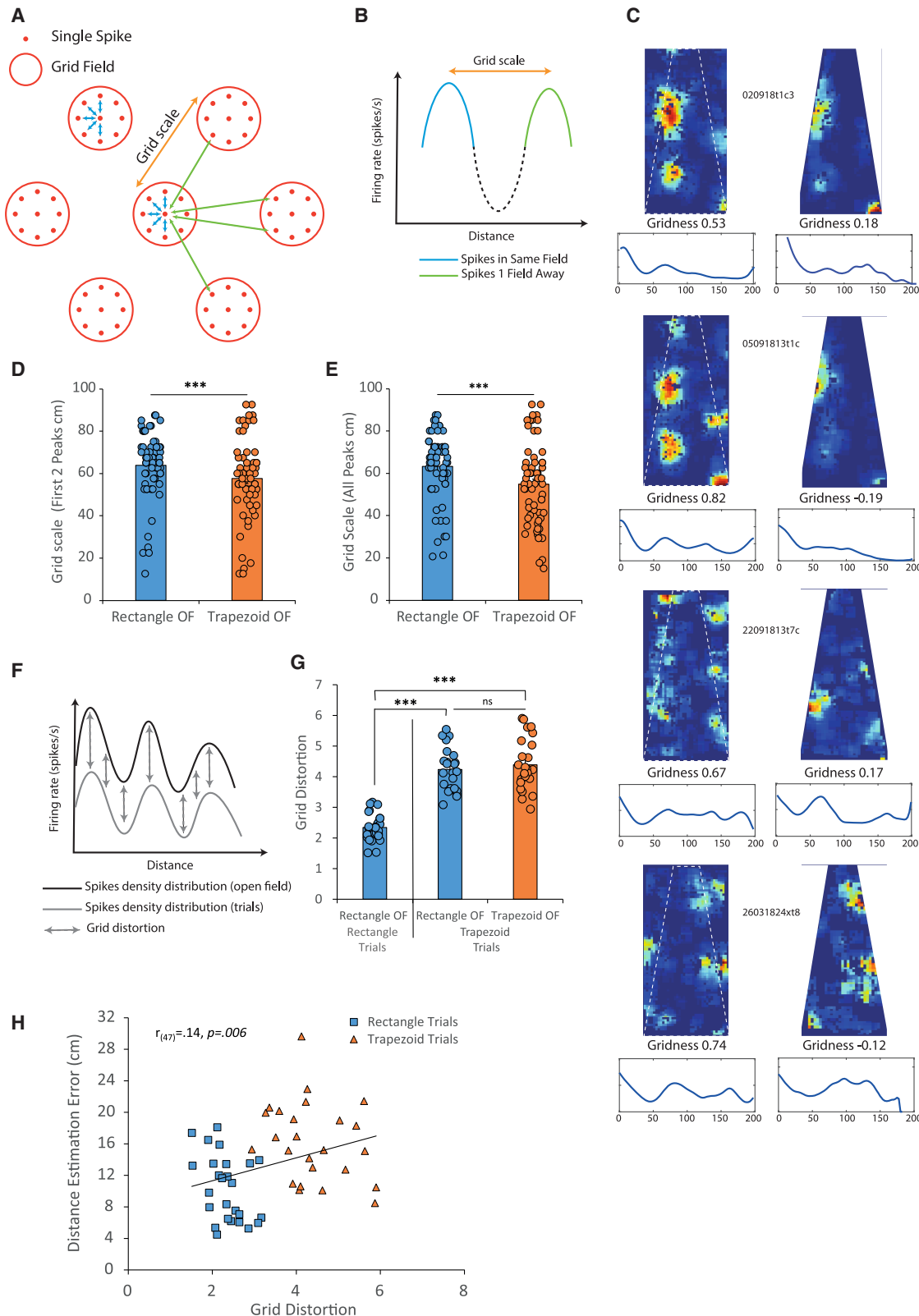
(F) Mean spatial information provided by grid cells in the rectangle and trapezoid open fields.

** $p < 0.01$. *** $p < 0.001$. n.s. indicates no significance. Error bars indicate \pm SEM.

See also **Figures S2** and **S3**.

Current Biology Report

CellPress
OPEN ACCESS



(legend on next page)

between grid distortion and distance estimation behavior, we correlated grid distortion from trials within a session with the average error in distance estimation. Consistent with a role for grid cell symmetry in path integration, there was a significant correlation between error and distortion, with greater levels of grid distortion being associated with more error in distance estimation (Figure 3H; $r_{(47)} = 0.14, p = 0.006$). To examine whether this effect holds within each condition, we carried out correlations of grid distortion and distance estimation for the rectangle and trapezoid trials separately. Neither of these correlations was significant, suggesting that the overall correlation is largely due to the significant group effect (rectangle trials: $r_{(47)} = -0.41, p = 0.38$, trapezoid trials: $r_{(47)} = -0.054, p = 0.799$). It is possible that variability in running trajectories or other behavioral noise within each condition, where the range of grid distortions is relatively narrow, may mask a subtle relationship between grid distortion and distance estimation errors. Future studies could attempt to better control behavioral variables across trials and/or record a larger number of grid cells to get a better estimate of grid distortion in each trial in order to probe this relationship further.

Grid regularity is affected by experience

Given the clear changes in grid structure induced by changing geometric features of the environment, we next asked whether grid structure would return to a regular and consistent pattern when rats returned to the standard rectangle configuration of the box. Interestingly, gridness score is still significantly lower in the second rectangle session relative to the first and indeed is not significantly different from the trapezoid session (Figures 4A and 4B; $\chi^2_{(2)} = 86.14, p < 0.001$; RECT1 vs. TRAP $p < 0.001$; RECT1 vs. RECT2 $p < 0.001$; reap vs. RECT2 $p = 0.435$). Given that the environment in the 2 rectangle sessions is identical, this argues against grid cells as supporting a universal spatial metric. It also suggests that we might expect a change in distance estimation behavior following exposure to the trapezoid environment. We examined this effect of experience on distance estimation in both the human and rodent versions of the task. The rat task was run with a pseudorandomized order of presentation of the rectangle and trapezoid. To test the effect of previous experience, we examined distance estimation in rectangle trials that were preceded by either a trapezoid or a rectangle trial. We found that there was no significant difference in distance estimation, suggesting that short experiences of the trapezoid

are not enough to impact later behavior in the rectangle ($W = 0.749, p = 0.688$; Figure S4A). However, as noted previously, the human version of the task was run in blocks, as the environment was too big to change configuration quickly enough for multiple changes in a session. Interestingly, this type of training gives more sustained experience of the trapezoid, similar in duration to the open field sessions in the rats, and so we might expect this to have a larger impact on distance estimation. To examine the effect of previous experience with the trapezoid on distance estimation in the rectangle, we looked at the trials in the first and second halves of the second block of rectangle trials that followed the block of trapezoid trials. In the first half of the trials in the rectangle following the trapezoid trials, we can see that distance estimation is significantly impaired relative to the first block of rectangle trials (Figure 4C; $F_{(1,495, 32.891)} = 9.013, p < 0.01$). This effect disappears in the second half of trials (Figure 4C; $F_{(2, 44)} = 6.034, p < 0.01$), showing that this effect is experience dependent and relatively short lived.

One further issue with the design is that both rats and humans were trained in the rectangle before being tested in both rectangle and trapezoid trials. It is possible that participants learn to estimate distance slowly over time and that the deficit in the trapezoid is the result of testing taking place earlier on that learning curve. To investigate this, we examined performance in the first and second halves of testing in both shapes (Figure S4). In humans there was a small but significant improvement in distance estimation over testing (Figure S4B, $t_{(22)} = 2.42, p = 0.024$; Figure S4C, $t_{(22)} = 3.67, p = 0.001$). The fact that this happens in both shapes, despite participants having more experience of the rectangle, argues against this being the result of greater familiarity with the rectangle. In rats, performance in the rectangle was not significantly different across the first and second half of testing in the rectangle ($t_{(15)} = 0.176, p = 0.863$; Figure S4D). However, performance in the trapezoid was significantly worse in the second half of testing relative to the first, despite levels of familiarity increasing ($t_{(15)} = 3.991, p = 0.0012$; Figure S4E). This suggests that increased experience of the trapezoid exacerbates distance estimation errors and argues against deficits in the trapezoid being due to a lack of experience, but future studies could examine whether rats trained in a trapezoid first would show similar patterns of behavior.

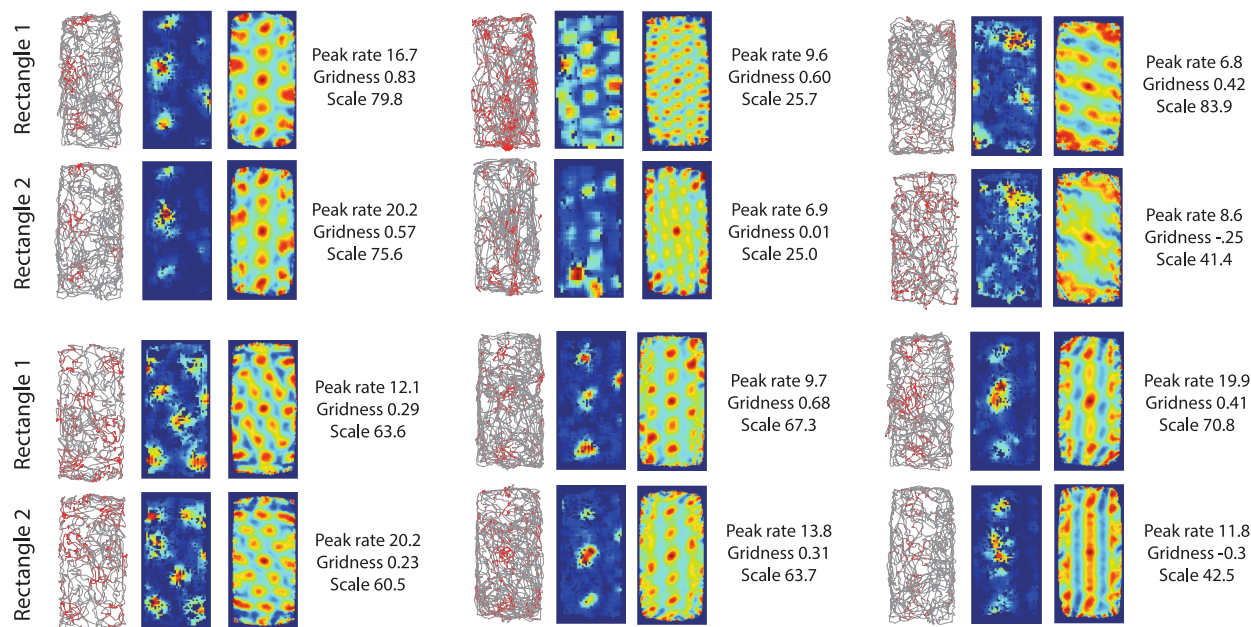
These combined findings show that symmetrical grid cell patterns in regularly shaped environments are affected by sustained experience in polarized environments like the trapezoid.

Figure 3. Decreased grid regularity is correlated with increased distance estimation error

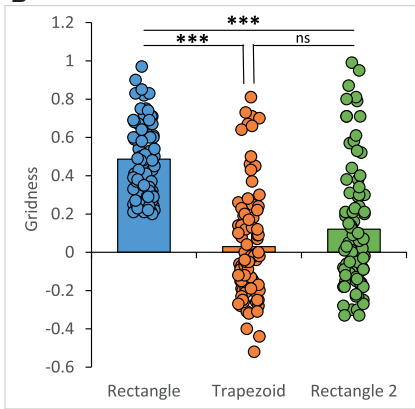
- (A) Diagram showing example Euclidean distances between pairs of grid cell spikes both within (blue lines) and between (green lines) grid fields.
- (B) Diagram of an example spike density distribution. Demonstrates the initial peak in density (blue) associated with intra-field spike density alongside a second peak in spike density (green) associated with inter-field spike density.
- (C) Rate maps (above) and spike density distributions (below) of grid cells in both the rectangle (left) and trapezoid (right) open fields. Dashed white lines show the outline of the trapezoid on the rectangle maps for reference.
- (D and E) Mean grid scale ($n = 67$) by computing the average distance between the spike density distributions (first 2 peaks or all peaks, respectively).
- (F) Diagram demonstrating how the distance between spike density distributions (grid distortion) is calculated for a given grid cell in the open field (black) and distance estimation trials (gray).
- (G) Mean difference in spike density distributions between the rectangle open field and the rectangle trials alongside the difference in spike density distributions between the trapezoid trials and both the trapezoid and rectangle open fields ($n = 67$).
- (H) Scatter plot, with line of best fit, showing the relationship between grid distortion (for a grid cell between the open field and the trials) and distance estimation error in both the rectangle (blue) and trapezoid (orange) trials.

*** $p < 0.001$. n.s. indicates no significance. Error bars indicate \pm SEM.
See also Figure S3.

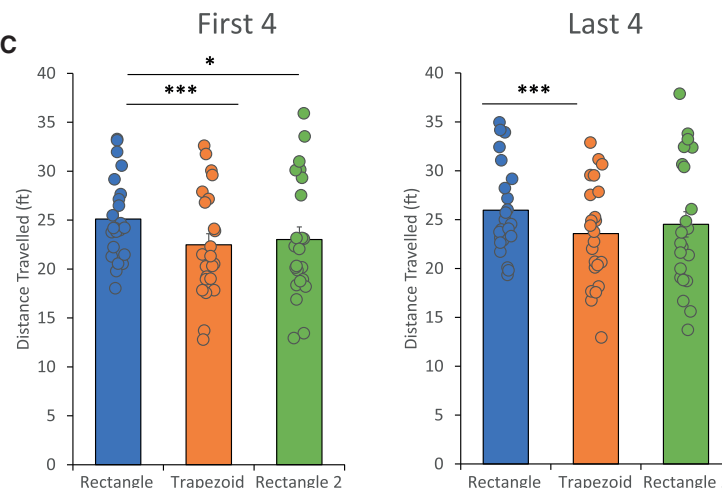
A



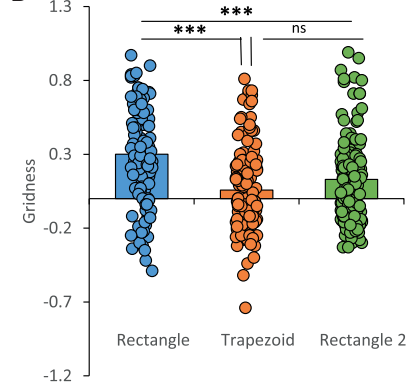
B



C



D



(legend on next page)

Consistent with this, sustained experience of the trapezoid also impacts distance estimation, while shorter experience does not. It is interesting to consider potential mechanisms that could support this. One possibility is that memory of previous experience modifies the grid signal and subsequent distance estimation behavior, potentially through decreasing the ability of the grids to learn about a changed environment. This could be mediated by hippocampal inputs into the deep layers of MEC, and so future studies could examine whether grids in the deep layers are more affected by experience than those in the superficial layers. However, it should be noted that the differences in the design between the human and rodent experiments (blocked vs. pseudorandom trials) make direct comparison difficult and also limit our ability to make strong conclusions across species. The findings are broadly consistent with prolonged exposure to trapezoids resulting in impaired distance estimation, while short-term exposure has no significant effect. Another possibility is that changes in spatial anchoring signals from other spatially modulated signals, such as border/boundary vector cells or object vector cells, caused by exposure to trapezoids, could underlie the experience-dependent distortion of grid cells in the rectangle. This could be examined in future studies of other types of spatially modulated signals.

Grid regularity is usually assessed using a gridness score that measures rotational symmetry relative to a distribution of gridness scores generated by shuffling spike timing and position data over multiple iterations. Using this measure, we initially reported 85 grid cells that passed the criterion of exceeding the 95th percentile in this shuffled distribution from the first rectangle session. However, it is also possible to classify grids based on the same shuffling procedure from the trapezoid and second rectangle session. Consistent with the previous findings, when we examine grid cells that pass the shuffling criterion in at least one of the open field sessions, we see a similar finding where gridness is significantly lower in both the trapezoid and the second rectangle session relative to the first rectangle session (Figure 4D; $\chi^2_{(2)} = 29.9, p < 0.001$; RECT1 vs. TRAP $p < 0.001$; RECT1 vs. RECT2 $p < 0.001$; REAP vs. RECT2 $p = 0.527$). This again suggests that grid representations are highly plastic and impacted by recent experience of polarized environments.

Grid cells in MEC have been widely discussed as a putative mechanism supporting a range of cognitive processes from large-scale allocentric cognitive maps to path integration. Here, we evaluate the suggestion that the highly symmetric and regular firing patterns of grid cells support the ability to accurately estimate distance traveled. Rats and humans were trained to run/walk a specific distance in real-world rectangular environments. Following training, distance estimation trials were carried

out in the rectangular environment and a trapezoid-shaped environment created by narrowing one end of the arenas. Rats and humans showed similar distance estimation errors in the trapezoid relative to the rectangle. This is consistent with previous findings of spatial memory errors in virtual reality, where errors in positional memory were shown to be increased in trapezoids relative to rectangles.²⁸ Exposure to the trapezoid was shown to produce distance estimation errors in subsequent trials in the rectangle in humans, suggesting that the mechanism used to support distance estimation is highly plastic and easily distorted. Next, we recorded from grid cells in MEC as rats carried out the same distance estimation task in both the rectangle- and trapezoid-shaped environments. Grid cells were distorted in the trapezoid, and this distortion was partially maintained in subsequent rectangle exploration sessions. Analysis of grid cells during distance estimation trials showed that distortion was again greater in trapezoid trials and that the level of distortion was significantly correlated with the amount of error in the distance estimation behavior across trial types. Within trial types, the correlations were not significant. This may be due to the relatively narrow range of distortions within each condition, which may be overshadowed by behavioral noise such as differences in trajectories.

Overall, these data are consistent with grid cells providing a distance estimation signal to support navigation in rats. This signal is easily distorted, which is consistent with reports of error signals in path integration.

RESOURCE AVAILABILITY

Lead contact

Further information and requests for resources and reagents should be directed to and will be fulfilled by the lead contact, James Ainge (jaa7@st-andrews.ac.uk).

Materials availability

This study did not generate new, unique reagents.

Data and code availability

- All data and code have been deposited on the University of St Andrews PURE website and are publicly available here: <https://doi.org/10.17630/82e80700-a40f-4521-ad77-9f422413458e>.
- Any additional information required to reanalyze the data reported in this paper is available from the [lead contact](#) upon request.

ACKNOWLEDGMENTS

J.A.A. is supported by BBSRC grant BB/X007197/1, and B.T. was supported by a BBSRC EastBio Studentship. D.B. is supported by a UKRI Frontier Research Grant (EP/X023060/1). In order to meet institutional and research funder open access requirements, any accepted manuscript arising shall be

Figure 4. Experience affects grid cell regularity

- (A) Spike maps, rate maps, and autocorrelations (left to right) for grid cells in the first (upper) and second (lower) rectangle open fields.
- (B) Mean gridness scores (cells defined by passing the gridness threshold in the first rectangle open field) in the first rectangle (blue), trapezoid (orange), and second rectangle (green) open fields ($n = 126$).
- (C) Mean distance traveled by humans ($n = 23$) in the first and second (left and right, respectively) halves of their distance estimation trials in the first rectangle (blue), trapezoid (orange), and second rectangle (green).
- (D) Mean gridness scores (cells defined by passing the gridness threshold in any of the open fields) in the first rectangle (blue), trapezoid (orange), and second rectangle (green) open fields.

* $p < 0.05$. *** $p < 0.001$. n.s. indicates no significance. Error bars indicate \pm SEM.

See also Figure S4.

open access under a Creative Commons Attribution (CC BY) reuse license with zero embargo.

AUTHOR CONTRIBUTIONS

Conceptualization, M.V.K. and J.A.A.; methodology, S.D., M.V.K., D.B., and J.A.A.; investigation, S.D., M.V.K., B.T., and J.A.A.; visualization, S.D., D.B., and J.A.A.; funding acquisition, J.A.A.; project administration, J.A.A.; supervision, J.A.A.; writing – original draft, J.A.A.; writing – review & editing, S.D., M.V.K., B.T., D.B., and J.A.A.

DECLARATION OF INTERESTS

The authors declare no competing interests.

STAR METHODS

Detailed methods are provided in the online version of this paper and include the following:

- KEY RESOURCES TABLE
- EXPERIMENTAL MODEL AND STUDY PARTICIPANT DETAILS
 - Rodent Trapezoid Experiment
 - Human Trapezoid Experiment
- METHOD DETAILS
 - Rodent Trapezoid Experiment
 - Human Trapezoid Experiment
- QUANTIFICATION AND STATISTICAL ANALYSIS
 - Rodent Trapezoid Experiment
 - Human Trapezoid Experiment

SUPPLEMENTAL INFORMATION

Supplemental information can be found online at <https://doi.org/10.1016/j.cub.2025.08.011>.

Received: February 23, 2025

Revised: June 10, 2025

Accepted: August 7, 2025

REFERENCES

1. Hafting, T., Fyhn, M., Molden, S., Moser, M.B., and Moser, E.I. (2005). Microstructure of a spatial map in the entorhinal cortex. *Nature* 436, 801–806. <https://doi.org/10.1038/nature03721>.
2. Buszaki, G., and Moser, E.I. (2013). Memory, navigation and theta rhythm in the hippocampal-entorhinal system. *Nat. Neurosci.* 16, 130–138. <https://doi.org/10.1038/nn.3304>.
3. Carpenter, F., Manson, D., Jeffery, K., Burgess, N., and Barry, C. (2015). Grid cells form a global representation of connected environments. *Curr. Biol.* 25, 1176–1182. <https://doi.org/10.1016/j.cub.2015.02.037>.
4. McNaughton, B.L., Battaglia, F.P., Jensen, O., Moser, E.I., and Moser, M.B. (2006). Path integration and the neural basis of the ‘cognitive map’. *Nat. Rev. Neurosci.* 7, 663–678. <https://doi.org/10.1038/nrn1932>.
5. Moser, M.B., Rowland, D.C., and Moser, E.I. (2015). Place cells, grid cells, and memory. *Cold Spring Harb. Perspect. Biol.* 7, a021808. <https://doi.org/10.1101/cshperspect.a021808>.
6. Tukker, J.J., Beed, P., Brecht, M., Kemper, R., Moser, E.I., and Schmitz, D. (2022). Microcircuits for spatial coding in the medial entorhinal cortex. *Physiol. Rev.* 102, 653–688. <https://doi.org/10.1152/physrev.00042.2020>.
7. Hales, J.B., Schlesiger, M.I., Leutgeb, J.K., Squire, L.R., Leutgeb, S., and Clark, R.E. (2014). Medial entorhinal cortex lesions only partially disrupt hippocampal place cells and hippocampus-dependent place memory. *Cell Rep.* 9, 893–901. <https://doi.org/10.1016/j.celrep.2014.10.009>.
8. Miao, C., Cao, Q., Ito, H.T., Yamashita, H., Witter, M.P., Moser, M.B., and Moser, E.I. (2015). Hippocampal remapping after partial inactivation of the medial entorhinal cortex. *Neuron* 88, 590–603. <https://doi.org/10.1016/j.neuron.2015.09.051>.
9. Rueckemann, J.W., DiMauro, A.J., Rangel, L.M., Han, X., Boyden, E.S., and Eichenbaum, H. (2016). Transient optogenetic inactivation of the medial entorhinal cortex biases the active population of hippocampal neurons. *Hippocampus* 26, 246–260. <https://doi.org/10.1002/hipo.22519>.
10. Allison, E.A.M.A., Moore, J.W., Arkell, D., Thomas, J., Dudchenko, P.A., and Wood, E.R. (2023). The medial entorhinal cortex is necessary for the stimulus control over hippocampal place fields by distal, but not proximal, landmarks. *Hippocampus* 33, 811–829. <https://doi.org/10.1002/hipo.23506>.
11. Allen, K., Gil, M., Resnik, E., Toader, O., Seeburg, P., and Monyer, H. (2014). Impaired path integration and grid cell spatial periodicity in mice lacking GluA1-containing AMPA receptors. *J. Neurosci.* 34, 6245–6259. <https://doi.org/10.1523/JNEUROSCI.4330-13.2014>.
12. Gil, M., Ancau, M., Schlesiger, M.I., Neitz, A., Allen, K., De Marco, R.J., and Monyer, H. (2018). Impaired path integration in mice with disrupted grid cell firing. *Nat. Neurosci.* 21, 81–91. <https://doi.org/10.1038/s41593-017-0039-3>.
13. Jacob, P.Y., Gordillo-Salas, M., Facchini, J., Poucet, B., Save, E., and Sargolini, F. (2017). Medial entorhinal cortex and medial septum contribute to self-motion-based linear distance estimation. *Brain Struct. Funct.* 222, 2727–2742. <https://doi.org/10.1007/s00429-017-1368-4>.
14. Parron, C., and Save, E. (2004). Evidence for entorhinal and parietal cortices involvement in path integration in the rat. *Exp. Brain Res.* 159, 349–359. <https://doi.org/10.1007/s00221-004-1960-8>.
15. Van Cauter, T., Camon, J., Alvernhe, A., Elduayen, C., Sargolini, F., and Save, E. (2013). Distinct roles of medial and lateral entorhinal cortex in spatial cognition. *Cereb. Cortex* 23, 451–459. <https://doi.org/10.1093/cercor/bhs033>.
16. Jacob, P.Y., Capitano, F., Poucet, B., Save, E., and Sargolini, F. (2019). Path integration maintains spatial periodicity of grid cell firing in a 1D circular track. *Nat. Commun.* 10, 840. <https://doi.org/10.1038/s41467-019-08795-w>.
17. Etienne, A.S., and Jeffery, K.J. (2004). Path integration in mammals. *Hippocampus* 14, 180–192. <https://doi.org/10.1002/hipo.10173>.
18. Tennant, S.A., Fischer, L., Garden, D.L.F., Gerlei, K.Z., Martinez-Gonzalez, C., McClure, C., Wood, E.R., and Nolan, M.F. (2018). Stellate cells in the medial entorhinal cortex are required for spatial learning. *Cell Rep.* 22, 1313–1324. <https://doi.org/10.1016/j.celrep.2018.01.005>.
19. Barry, C., Hayman, R., Burgess, N., and Jeffery, K.J. (2007). Experience-dependent rescaling of entorhinal grids. *Nat. Neurosci.* 10, 682–684. <https://doi.org/10.1038/nn1905>.
20. Hardcastle, K., Ganguly, S., and Giocomo, L.M. (2015). Environmental boundaries as an error correction mechanism for grid cells. *Neuron* 86, 827–839. <https://doi.org/10.1016/j.neuron.2015.03.039>.
21. Stensola, H., Stensola, T., Solstad, T., Frøland, K., Moser, M.B., and Moser, E.I. (2012). The entorhinal grid map is discretized. *Nature* 492, 72–78. <https://doi.org/10.1038/nature11649>.
22. Boccara, C.N., Nardin, M., Stella, F., O’Neill, J., and Csicsvari, J. (2019). The entorhinal cognitive map is attracted to goals. *Science* 363, 1443–1447. <https://doi.org/10.1126/science.aav4837>.
23. Butler, W.N., Hardcastle, K., and Giocomo, L.M. (2019). Remembered reward locations restructure entorhinal spatial maps. *Science* 363, 1447–1452. <https://doi.org/10.1126/science.aav5297>.
24. Chen, G., Manson, D., Cacucci, F., and Wills, T.J. (2016). Absence of visual input results in the disruption of grid cell firing in the mouse. *Curr. Biol.* 26, 2335–2342. <https://doi.org/10.1016/j.cub.2016.06.043>.

25. Krupic, J., Burgess, N., and O'Keefe, J. (2012). Neural representations of location composed of spatially periodic bands. *Science* 337, 853–857. <https://doi.org/10.1126/science.1222403>.
26. Krupic, J., Bauza, M., Burton, S., Barry, C., and O'Keefe, J. (2015). Grid cell symmetry is shaped by environmental geometry. *Nature* 518, 232–235. <https://doi.org/10.1038/nature14153>.
27. Krupic, J., Bauza, M., Burton, S., and O'Keefe, J. (2018). Local transformations of the hippocampal cognitive map. *Science* 359, 1143–1146. <https://doi.org/10.1126/science.aao4960>.
28. Bellmund, J.L.S. (2020). Piecing together cognitive maps one dimension at a time. *Neuron* 107, 996–999. <https://doi.org/10.1016/j.neuron.2020.08.014>.

STAR★METHODS

KEY RESOURCES TABLE

REAGENT or RESOURCE	SOURCE	IDENTIFIER
Chemicals, peptides, and recombinant proteins		
Cresyl-violet	Sigma	Cat #C5042
Deposited data		
Dataset	This paper	https://doi.org/10.17630/82e80700-a40f-4521-ad77-9f422413458e
Experimental models: Organisms/strains		
Rat: Lister Hooded	Envigo	Strain: HsdOia:LH
Software and algorithms		
TINT: Spike sorting software	Axona	http://www.axona.com
MATLAB	Mathworks	https://www.mathworks.com/products/matlab
IBM SPSS Statistics	IBM	https://www.ibm.com/products/spss-statistics
JASP Statistics	JASP	https://jasp-stats.org/
GraphPad Prism Statistics	Dotmatics	https://www.graphpad.com/
Other		
Axona Re-usable Microdrive	Axona	http://www.axona.com/
Axona Digital Acquisition System	Axona	http://www.axona.com/
Gold Plating Solution	Neuralynx	https://neuralynx.fh-co.com/
17 um Platinum Iridium Wire	Axona	http://www.axona.com/

EXPERIMENTAL MODEL AND STUDY PARTICIPANT DETAILS

Rodent Trapezoid Experiment

21 experimentally naive male lister hooded rats (Envigo, UK) were the subjects of this study. They were housed in groups of three and testing took place in the light phase of a 12-hour light/dark cycle. During behavioral testing rats were kept on a restricted diet of 20g per rat per day with unlimited access to water and were monitored to assure they did not drop below 85% of their free-feeding body weight. This study was performed in line with both national and international legislation for the testing and maintenance of laboratory animals (Animals [Scientific Procedures] Act, 1986; European Communities Council Directive 2010 [2010/63/EU] and under the project licence of Professor James Ainge (PPL7018306/P53E784C4).

Human Trapezoid Experiment

A total of 23 participants took part in the study (15 female, mean age = 23.4 years, SD = 3.3, range: 19–30 years), that was approved by the University of St Andrews Teaching and Research Ethics Committee. All participants were paid £7 for their participation in the experiment.

METHOD DETAILS

Rodent Trapezoid Experiment

Apparatus

Testing took place within a rectangular box (190cm x 90cm) which could be transformed into a trapezoid (Figure 1A). In the trapezoid configuration, the long walls maintained their 190cm length; however, while the box was fixed at 90cm wide at one end, the two long walls converged to form 20cm wide wall at the far end. There was a smaller starter box linked to the wider end of the box by a trap door. The experimenter sat behind this start box throughout training and testing. Sand was spread around the entirety of the box and moved around between trials and phases to prevent the use of olfactory/visual cues from the floor of the environment. There were several global cues visible from within the testing box. Additionally, strips of tape were placed on the floor outside the box (not visible from inside) to indicate goal distances to the experimenter (Figure 1A – black dashed lines indicate goal zone). Each session was recorded by a camera placed directly above the box allowing for a bird's eye view of behavior within the box.

Behavioral Procedure

The 21 rats were trained in two cohorts. A behavioral cohort of 16 animals were trained and tested first, followed by an electrophysiology cohort of 5 animals.

Habituation. Rats were first habituated in cage groups for 20 minutes twice a day for two days. On each day they were habituated to each environment in one of the two 20-minute sessions. Next, rats were habituated individually for 10 minutes in each environment, daily, for a further two days.

Training. Training consisted of four phases all completed in the rectangular configuration of the box. Rats progressed to the next phase of training when they had successfully completed all trials within 30 minutes on two consecutive days. In phase 1 rats completed 20 baited trials where a quarter weeto was placed in the middle of the goal zone (the goal zone was 123-138cm from the start box door). The start box door was opened, and the rat allowed into the testing box to find the weeto. Once they had eaten the weeto the start box door was re-opened and a full weeto dropped into the start box to encourage the rat to return. When the rat returned to the start box, the door 3 was closed, and the rat allowed to eat the reward weeto. The trial was then reset by moving the sand around inside the test box and placing another quarter weeto in the goal zone.

Phase 2 consisted of the same procedure as phase 1; however, only the first 10 of a total of 20 trials were baited with a quarter weeto. In unbaited trials the rat was required to run from the fixed wall (where the start box door was located) to the reward zone and pause for a second. At this point a full weeto was dropped into the start box and the door opened allowing the rat to complete the trial.

In phase 3 the procedure was identical to phase 2; however, rats ran only 15 trials: 5 baited followed by 10 unabated. In phase 4, rats simply ran 10 unbaited trials.

Of course, rats did not always complete the trials correctly on the first attempt. Therefore, if the rat mis-estimated the distance to the goal zone on the first attempt, following attempts were classified when the rat returned to the fixed wall before attempting to run to the goal zone once again.

Testing. During testing, each rat first performed two baited ‘reminder’ trials, where a quarter weeto was placed in the center of the reward zone (as in training). These reminder trials were not included in analysis of distance estimation behavior. Rats then performed 10 unbaited trials – 5 in the rectangle and 5 in the trapezoid (Figure 1A). The order of rectangle and trapezoid trials was pseudo-randomized. In test trials the goal zone was expanded from 123-138cm to 111-149cm (Figure 1A – indicated by black dashed lines in box diagram) in order to allow for any potential over/underestimation of distance as a result of the changing environmental geometry. Testing then took place over 8 days.

A group of five implanted animals performed an extended testing session consisting of four phases to allow for electrophysiological recording. In the first two phases the rats explored the rectangle and trapezoid open fields respectively for 10-15 minutes (Figure 2A). Quarter weetos were thrown into the testing box to encourage exploration of the whole environment. The third phase consisted of the distance estimation task described above. Finally, in the fourth phase the rats explored the rectangle for a further 10-15 minutes.

Surgery

Five rats were implanted with steel micro-drives (Axona, UK). Microdrives were prepared with 8 tetrodes threaded through a 20-gauge steel canula and secured to the drive with dental cement. Tetrodes were made of 4 electrodes of 17 μ m in diameter (composed of a platinum (90%) iridium (10%) complex) twisted around each other. The tips of these electrodes were gold-plated to achieve an impedance of 100-300k Ω on the day of surgery. These drives were then implanted unilaterally into mEC layer II. Rats were first anesthetized using 2L/min oxygen with 5% isoflurane (Abbott Laboratories, Maidenhead, UK) in an induction box. Rats were then placed in a stereotaxic frame (David Kopf Instruments, Tujunga, CA) and anesthesia maintained at 2-3% isoflurane and 1.2L/min oxygen, via a facemask. The analgesic – injectable Metacam – was injected subcutaneously (0.05ml/rat) and the rat’s head shaved. An incision was then made along the midline of the scalp to expose the skull and the constituent landmarks (midline, bregma and lambda). These landmarks were used to ensure the skull was level. Holes were then drilled in the skull for between 5 and 7 skull screws to allow the implant to be secured to the skull with dental cement later. A ground wire was attached to one of these screws and later soldered to the ground wire on the microdrive. Microdrives were then implanted into left mEC (ML – 4.5mm; AP – 0.4mm from the anterior edge of the transverse sinus; DV - 2.5mm). The electrodes were then angled at 10 and inserted into layer II of mEC. The craniotomy around the electrodes was then filled with Vaseline before the entire implant was secured onto the skull surface using dental cement with the skull screws as anchoring points. Rats were then placed in a heated box to recover from anesthesia and were closely monitored during their recovery from surgery throughout the following 48 hours.

In-vivo Electrophysiological Recordings

Recordings signals were taken from microdrives through a series of amplifiers (AXONA Ltd, UK) to a desktop PC, running specialized digital data acquisition software (DACQ – AXONA Ltd, UK) by a cable suspended above recording arena. The signal was amplified 5000-20000 times and bandpass filtered (600–6,000 Hz). An EEG signal was also monitored to detect theta rhythm (6-12 Hz) - a characteristic local field potential found in the hippocampus and surrounding areas. Two infrared lights atop the microdrive allowed the acquisition software to track the position of the animal within the environment using the IR camera above the box.

Behavioral Analysis

Distance estimates were scored offline using video recordings from a camera above the testing arena. Average distance travelled by rats in each condition was calculated by measuring the distance between the start box door and the distance at which the animal halted to indicate its estimate. Furthermore, the absolute difference between the distance to the center of the goal zone

(130.5cm; where the weeto was placed during baited training and reminder trials) and the distance travelled by the rats was also calculated, as a measure of distance estimation error. The mean errors for both environmental configurations were calculated.

Analysis of Electrophysiological Recordings

Waveforms recorded during exploration and trial phases for each session, were first analyzed in a specialized cluster cutting program – Tint (Axona, UK). Waveforms were first placed into groups putatively originating from the same neuron through principal component analysis (through Klustakwik, Tint function). The results of this grouping were then manually examined to ensure groups of similar waveforms had not been mistakenly separated by the program and also to ensure groups of different waveforms had not been merged. Efforts were also made to remove as much noise (waveforms clearly not originating from neurons) as possible to allow for a clean signal.

Grid Cell Identification. Those groups of waveforms from putative grid cells were then analyzed to produce a gridness score using the method first described by Hafting et al.¹

First, rate maps were produced for each grid binning the positional data into 2.5x2.5cm bins. The number of spikes, and time spent, in each bin were then determined producing spike and dwell time maps. Spikes fired when the animal was moving at less than five meters per second were not included in analyses. These maps were then smoothed using a 5x5-bin boxcar filter. The number of spikes for each bin was divided by the dwell time of that bin in order to produce a rate map.

Spatial autocorrelations were then produced for each putative grid map. Using this map, a gridness scores was then produced by assessing the rotational symmetry of the central 6 peaks of the autocorrelogram. A cell was classified as a grid cell if its gridness score was greater than both 0.2 and 95% of a shuffled distribution of gridness scores. This distribution was generated for each grid cell by randomly shuffling spike times and positions, by a minimum of 30 seconds, 1000 times.

Quantification of Spatial Information. The spatial information score of each unit was calculated using the following formula (as described by: Skaggs & McNaughton, 1993)

$$\text{Spatial Information} = \sum_i P_i \frac{\lambda_i}{\lambda} \log_2 \frac{\lambda_i}{\lambda} \quad (\text{Equation 1})$$

The information about current location encoded in each spike is calculated in bits/spike. In this formula P_i is the probability that the animal is currently in bin i , λ is the average firing rate for that unit and λ_i is the average firing rate in bin i .

Euclidean Spike Distance Distributions. Euclidean distance distributions were produced for each cell through measuring the Euclidean distance between each pair of spikes fired by a given grid cell in a session (Figure 3A). Distributions were calculated for both the open-field sessions and for the rectangle/trapezoid trials. The number of spikes per second (i.e. firing rate) per 2.5cm distance increment was then plotted to produce a Euclidean inter-spike distance distribution (or a spike density distribution; Figure 3B). For a given grid cell this distribution shows a peak at very short distances (see blue portion of distribution in Figures 3A and 3B), as for any given grid cell spike, there will likely be many spikes in proximity, that share the same grid field. Then, as the distance increases and moves into the area between grid fields, the firing rate will decrease dramatically as few spikes will be this distance apart (see dashed portion of distribution in Figure 3B). As distance further increases, the firing rate will increase once more (see green portion of distribution in Figures 3A and 3B) as there will be many spikes that are separated by the distance between grid fields. Thus, the distance between peaks in the spike density distribution will mirror the scale of the grid. These spike density distributions were produced for each cell in each session/set of trials.

The pairwise distance between spike density distributions for each grid cell in the rectangle or trapezoid trials and the respective open field sessions were calculated (Figure 3C). For each 2.5 cm increment in distance (x-axis - Figure 3C), the distance between the distribution for the grid in the open field (blue line in Figure 3C) and the distribution for the same grid in the rectangle or trapezoid trials (red line in Figure 3C) was calculated (dashed line arrows in Figure 3C). The median distance between distributions was then calculated to assess the extent to which firing patterns retained their periodicity between the trials and their respective open-field sessions. The larger the distance between these distributions the greater the distortion in periodicity between the open field and trials sessions. We will hereon, refer to this as ‘grid distortion’.

For the comparison of spike density distributions between the trials and open-field sessions distributions were calculated for 100cm instead of the full 190 cm length of the testing box. This was done as rats did not travel the full 190cm length of the box in any given trial, meaning there were no spike pairs 190cm apart. Furthermore, with an average grid scale of 82.5cm (SD = 9.87cm) and a maximum scale of 100.7cm, a comparison of spike density distributions for the first 100cm was sufficient to encapsulate a minimum of 2 fields for each grid cell.

We also examined the distances between the peaks of these spike density distributions to assess the relationship between these one-dimensional distributions and the more traditionally used two-dimensional rate maps.

Histology

Animals, from whom grid cell recordings were obtained, were transcardially perfused following a lethal dose of pentobarbital through IP injection. Perfusion was carried out with ~100ml of phosphate-buffered saline (PBS) followed by ~350ml of 4% paraformaldehyde (PFA). Brains were stored in 20% sucrose solution (in PBS) for 24 hours at 4°C, following extraction. A freezing microtome was then used to section brains into 50μm sagittal sections, before being mounted on glass slides and fixed in a PFA bath overnight.

Cresyl-Violet Staining. Mounted sections were then stained with cresyl-violet solution to increase the visibility of the electrode tracts. Sections were first placed in a PFA bath overnight. Each slide was submerged in xylene before being submerged in two ethanol solutions in 100% and 50% respectively before a water bath. Slides were then placed in cresyl-violet solution for 2mins

before being washed in running water for 5 mins. Finally, the slides were placed back in the ethanol and xylene solutions in reverse order before the slides were then cover-slipped with DPX mounting solution.

Human Trapezoid Experiment

Apparatus

The experiment took place in a section of Club 601, a nightclub located in the University of St Andrews Student's Union. This venue was chosen as it was large enough to set up the arena, had distinct features around the periphery of the room serving as external, global landmarks and a high ceiling, which meant there were no obvious cues directly overhead any potential area within the arena.

The rectangular arena was 40 feet (12.2m) long by 20 feet (6.1m) wide by 7 (2.1m) tall constructed with four timber frame flats (50mm x 20mm; Rembrand Timber, UK) – two long flats (40 feet / 12.2m long by 7 feet / 2.1m tall) and two short flats (20 feet / 6.1m long by 7 feet / 2.1m tall; see [Figure 1D](#)).

The flats stood upright with the help of timber braces held down by stage weights. The four flats were fixed to each other using removable pin hinges (Flints Hire and Supply, UK). A black roscotex molton exhibition fabric (J. D. McDougall, UK) was stapled over each of the four timber frames, thus providing opaque walls. The molton fabric was specifically chosen as it absorbed light without casting shadows inside the arena. A small door was installed on one of the short flats to allow entry in and exit out of the arena. The floor of the room was lined with black polythene sheeting plastic covers (Elixir, UK) and sprinkled with dust-free wood shavings (Bedmax, UK). Cameras were placed at either end of the arena to record participants during the experiment.

To transform the rectangular arena into a trapezoid, two ends of the long flats were moved inwards. The flats were light enough that two people were able to physically lift and move them in to place. A separate flat (1.4m long by 2.1m high) was slipped in and attached to the ends of the long flats using pin hinges to form the shorter back wall of the trapezoid.

Design

The study design consisted of two habituation phases – starting with the rectangle and then the trapezoid – followed by a training phase in the rectangle and then three testing phases in the rectangle, trapezoid and rectangle respectively. The purpose of having a second rectangle test phase at the end was to check if any potential alteration in distance estimation in the trapezoid was genuine and not merely a result of poor task encoding during the training phase.

Procedure

Throughout training and testing the experimenter stood off center against the wall of the arena which contained the door, in order to provide no distance cues to the participants that were not already provided by the wall itself. Before participants arrived, the rectangular arena was set up for the habituation phase. The set-up included placing nine poster tubes along the perimeter of the arena and one tube right in the center with a colored plastic ball on top of each tube. Participants were made to stand in the middle along one of the short walls they had just entered through the door. A tape marking on the floor indicated the starting position participants needed to stand behind. Participants were instructed to pick up one colored ball at a time and deposit each one individually into an empty poster tube located next to them behind the starting position. Participants were told that the order in which they picked the balls was irrelevant to the task. The only requirement was for them to walk as normally and naturally as they would in a natural setting. The purpose of having balls located in specific areas along the walls of the arena was to control the locations that all participants visited within the arena and also to familiarize them with its geometry.

At the end of the first habituation phase, participants were asked to turn around and face the wall and were provided with a blindfold that they were requested to put on. The use of the blindfold was to replicate the time when rats were in the starter box as changes were made to the testing box. The experimenter started playing music (Spotify) from a laptop next to the participant before changing the arena to a trapezoid and resetting the balls and poster tubes. Each arena change took an average of five minutes across all phases. Music was played to keep the participant engaged while also providing a mask for sounds related to moving the arena. Once the trapezoid arena was reset, participants were made to complete an identical habituation session.

In preparation for the training phase, poster tubes and balls were removed from the rectangular arena while the participant was blindfolded. A bar stool with high back was placed in a straight line 25.5 feet away from the participant. Participants were given 10 trials during the training phase. For each trial, participants would remove their blindfold and turn and face the front where they could see the chair. They would then walk normally and naturally, as practiced during habituation, in a straight line until the front of their body touched the back of the chair. Participants were asked to put their hand up and acknowledge that they had reached the designated point and pause of a couple of seconds before returning back. Participants were required to count aloud backwards in 7s from a three-digit number assigned to them at the start of each trial. They did this on their way both to and from the chair. The purpose of this articulatory suppression task was to prevent participants from counting the number of steps between their starting position and the chair. At the end of each trial, participants turned back to face the wall and put on the blindfold. In between trials, the experimenter would walk up to the chair and make an obvious attempt at moving the wood shavings around. This took approximately 10-15 seconds.

During test phases, the chair was removed from the arena. Across eight trials, participants were asked to walk normally and naturally up to where they had previously stopped when the chair had been in the arena. The only other difference in the test phases was that, at the end of each trial, participants were asked to report how confident they were at having replicated the practiced distance. This was done on the same laptop playing music between arena changes. Across habituation, training and testing phases, participants were not given specific instructions about what to pay attention to within the arena or the room (e.g. landmarks, the back wall etc.). The only consistent instruction was to walk as they would in an everyday setting.

Behavioral analysis

Distance estimates made by participants were scored offline. A screen ruler (<http://www.softpedia.com/get/Desktop-Enhancements/Other/Desktop-Enhancements/Programs/Screen-Ruler.shtml>) was used to measure the on-screen distance in pixels, which was then converted to feet travelled in the arena. When scoring videos using footage from the camera at the near end, distance traveled was calculated by measuring the distance between the front of the participants shoes at the point they made their distance judgment and the base of the far wall and then subtracting that from the total length of the arena. For videos taken with the camera at the far wall, distance was measured from the starting tape at the near wall to the front of the participants shoes when they stopped to make their distance judgment. These two distance values were then averaged to give a final measure of distance estimated.

QUANTIFICATION AND STATISTICAL ANALYSIS

ARRIVE guidelines were followed to ensure rigor and reproducibility. The studies had a within subject design with subjects providing their own control conditions through comparison of performance and neural signals across different conditions. No exclusion criteria were used and all participants completed testing. No randomization was necessary due to the within subjects nature of the study. Experiments and analysis were run blind where possible and where not possible were scored by a blind researcher to check for consistency.

Rodent Trapezoid Experiment

Statistics were calculated in JASP and GraphPad Prism. Differences in distance traveled and distance estimation error were assessed using 2x2 (geometry vs landmarks) repeated measures ANOVAs with Bonferroni corrected post-hoc tests. Differences in distance estimation error in the electrophysiology cohort were assessed using a paired t-test. Due to parametric assumptions not being met, Wilcoxon Signed Rank tests were used to assess the differences in gridness score, information score and number of fields for grid cells between the rectangle and trapezoid open-fields. Kruskal Wallis tests in combination with Dunn's Post-Hoc tests were used to assess differences in grid distortion. A Pearson's correlation was used to assess the relationship between grid distortion and distance estimation error.

Human Trapezoid Experiment

Statistics were calculated in SPSS. One way repeated measures ANOVAs (rectangle 1 vs. trapezoid vs. rectangle 2) were conducted to investigate the effect of environmental geometry on distance estimated. A Greenhouse-Geisser correction was applied in scenarios when the assumption of sphericity was violated. Where *post hoc* analyses were conducted, a Bonferroni adjustment was applied.